**Preprints of the 19th World Congress**
**The International Federation of Automatic Control**
**Cape Town, South Africa. August 24-29, 2014**

# A Reduced Order Model of the Indoor-Air Environment for Energy Efficient Building Studies

**Samah Ben Ayed** * **Jeffrey T. Borggaard** ** **Eugene M. Cliff** ***

* *Interdisciplinary Center for Applied Mathematics, Virginia Tech, Blacksburg, VA 24061 USA (e-mail: samah09@vt.edu).*
** *(e-mail: jborggaard@vt.edu)*
*** *(e-mail: ecliff@vt.edu)*

**Abstract:** Computational fluid dynamics (CFD) is used to generate dynamic response data for the temperature and moisture distributions in a restaurant. We present a procedure for developing a reduced order model (ROM) by formulating a linear time-invariant (LTI) model that approximates the perturbations recorded in the CFD responses. An overall system model would include the ROM model of the indoor-air environment along with models for the dynamics of the building envelope and for the mechanical equipment. Here we include a simple model for the building envelope and demonstrate an optimal control problem.

*Keywords:* energy efficiency, dynamic model, model predictive control

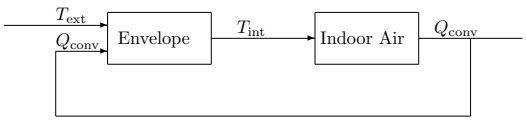


Fig. 1. Envelope Indoor-Air Coupling

## 1. INTRODUCTION

Approximately 40% of global energy is expended in buildings to support heating-ventilation-air-conditioning (*HVAC*), lighting, and plug loads. Even modest reduction in this use represents significant contributions toward relief of a host of pressing environmental issues. Here we focus on cooling requirements and specifically on the development of models for predictive control of the indoor environment.

Energy flow in buildings evolves on multiple time and spatial scales including exchange between the exterior environment/building shell, conduction through the shell, and convection/radiation on interior surfaces. In this paper we study energy exchange on the interior surfaces, although the ideas can be applied to exterior heat transfer.

The basic coupling between the building envelope and the indoor-air is represented in Fig. 1. Here $T_{\text{int}}$ ($T_{\text{ext}}$) is the temperature on an indoor surface (outdoor surface), and $Q_{\text{conv}}$ is the convective heat load from indoor-air to the surface (w/m$^2$). The simplest and most commonly used mathematical model is

$$Q_{\text{conv}}(t) = h\left(T_{\text{air}}(t) - T_{\text{int}}(t)\right) \ , \tag{1}$$

where $T_{\text{air}}$ is a *zone air temperature*, $h$ is a Newton film-cooling coefficient, and $Q_{\text{conv}}, T_{\text{int}}$ are averaged values over some part of the interior surface. Such models are commonly used in energy simulation codes, such as EnergyPlus where the value of the film coefficient is computed from experimental correlations based on surface composition and orientation among other factors.

One may choose to directly formulate a coupled model wherein the solid conduction (the envelope) and fluid convection (the indoor-air) are analyzed simultaneously - a problem of *conjugate heat transfer*. Various approaches to couple prediction codes for fluid dynamics and solid conduction have also been studied (Srebric (2000) and Zhai (2002)). Our purpose here is to construct a reduced-order model (Borggaard (2012), Gugercin (2008) and Kung (1978)) suitable for use in studies of model predictive control (Ma (2012)).

## 2. CFD-BASED MODEL

Our approach to developing a reduced-order model is to construct a linear time-invariant (LTI) model that approximates the input-output behavior observed in computational fluid dynamics (CFD) simulations. Accordingly, a CFD model was developed based on FLUENT. As indicated in Fig. 1, coupling between the indoor-air and the envelope models is naturally achieved by treating the bounding surface temperatures as inputs to the CFD and the corresponding surface heat fluxes as outputs; that is, we approximate the Dirichlet-to-Neumann (dynamic) response. Other CFD inputs include the mass-rate, temperature, and humidity supplied by the roof-top-units (RTU), the sensible and latent loads provided by occupants, and external loads from kitchen airflow. Additional outputs of interest include air temperature/humidity at selected zones/locations, and return air properties.

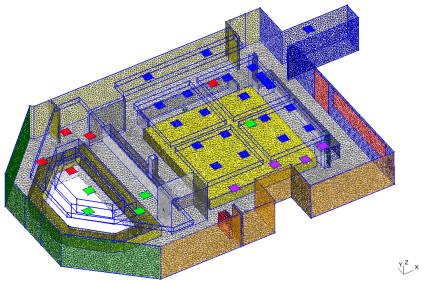

Fig. 2. Grid with zones - the left (green) wall is North

### 2.1 Nominal Boundary/Source Conditions

The indoor-air response is decomposed into a nominally steady part and a perturbation. For the steady part we apply fixed boundary and source conditions enumerated here:

*Bounding Surfaces*; For five of the bounding surfaces we prescribe no-slip flow and fixed temperature (Dirichlet) data

- North Wall: 27.00$^o$C
- East Wall: 25.58$^o$C
- West Wall: 28.43$^o$C
- Floor: 24.92$^o$C
- Ceiling: 25.48$^o$C

*Kitchen Interface*: The south wall boundary of our computational domain (see Fig. 2) separates the dining zone from the kitchen, which is not modeled. For the solid part of this boundary we impose no-slip flow and adiabatic thermal conditions. For the opening(s) between the kitchen and the dining zones we have prescribed flow from the kitchen.

- mass-rate: 0.591 kg.s
- temperature: 25.00$^o$C
- water mass-fraction: 16 g/kg

*Supply Air*: Each supply air vent is a 2 ft by 2 ft ceiling mounted square. The air supply from each RTU is uniformly distributed among the associated vents, and is supplied at 16.60$^o$C. The velocity at each vent is normal (*i.e.* downward), and is spatially distributed using a flattened parabolic profile.

- RTU#1- mass-rate: 2.9320 kg/s; water mass-fraction 7 g/kg; distributed over 19 supply vents (blue)
- RTU#2- mass-rate: 0.5320 kg/s; water mass-fraction 9 g/kg; distributed over 04 supply vents (red)
- RTU#3- mass-rate: 0.3990 kg/s; water mass-fraction 9 g/kg; distributed over 03 supply vents (purple)
- RTU#4- mass-rate: 0.5320 kg/s; water mass-fraction 9 g/kg; distributed over 04 supply vents (green)

Note that RTU#3 supplies four vents but only three of these are in the computational domain.

*Return Air*: Each of the return vents is ceiling mounted. These are specified as *pressure outlet* with the flow normal to the boundary, and the pressure at 40 Pa below that on the floor. The pressure difference approximates the static head loss under vertical equilibrium (*i.e.* $\Delta P = -\rho\, g\, \Delta h$) at a ceiling height of 3.4 m (one return per RTU).

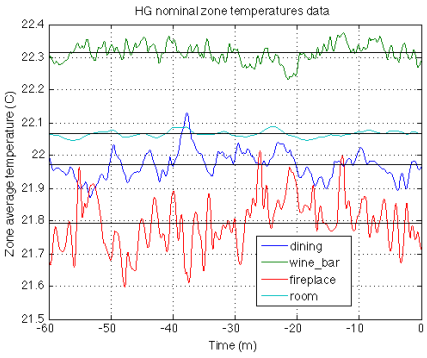


Fig. 3. Steady response; Zone Average Temperatures

*Dining Area Source*: The dining area is the roughly 69 m$^3$ volume shown in yellow in Fig. 2. The intent is to simulate the sensible/latent loads produced by the occupants. In this volume we uniformly distribute an energy source of approximately 8,750 w, and a moisture source of approximately 3.08 g/s.

*Wine Bar Area Source*: The winebar area is the roughly 23 m$^3$ volume that surrounds the winebar. The intent is to simulate the sensible/latent loads produced by the occupants. In this volume we uniformly distribute an energy source of approximately 3,310 w, and a moisture source of approximately 1.10 g/s.

## 3. STEADY STATE RESPONSE

The system was subjected to fixed boundary and source conditions chosen to represent a mean condition in the space (see § 2.1). FLUENT was run in both steady and unsteady modes; the latter consisted of seven hours of simulated time with external (boundary & source) conditions fixed. Some responses for the last hour are shown in Figures 3. The black horizontal lines are averages over the one-hour window. The meaning of these various temperatures can be understood in terms of Fig. 2. In particular

- **dining zone** is the yellow rectangular volume in the center of the figure
- **wine_bar zone** is the yellow volume in the shape of a reflected **D** in the left of the figure
- **fireplace** is the surface of the red box in the left foreground (to the left of the entrance *bump-in* )

Note that the *room average* is the least oscillatory: it is the mass-averaged temperature over the entire room. The *dining* and wine_bar values are mass-averaged over the cited volumes. The *fireplace* value is averaged over the external surfaces of the designated red-box, and exhibits the largest oscillations. Also, note that the values at the *right* end ($t = 0$) do not generally match the average, and this is particularly noticeable in the *fireplace* data. One might expect that the oscillations would decay and the internal flow in the room would become steady. In fact there is no guarantee that a steady flow exists, moreover the computed results depend on the grid which is likely somewhat too coarse.

| Number | Name | Nominal Value | Increment |
|---|---|---|---|
| 1 | north_temp | 27.00$^o$C | 5.00$^o$C |
| 2 | east_temp | 25.58$^o$C | 5.00$^o$C |
| 3 | west_temp | 28.43$^o$C | 5.00$^o$C |
| 4 | floor_temp | 24.92$^o$C | 5.00$^o$C |
| 5 | ceiling_temp | 25.46$^o$C | 5.00$^o$C |
| 6 | rtu_1_temp | 16.60$^o$C | −5.00$^o$C |
| 7 | rtu_2_temp | 16.60$^o$C | −5.00$^o$C |
| 8 | rtu_3_temp | 16.60$^o$C | −5.00$^o$C |
| 9 | rtu_4_temp | 16.60$^o$C | −5.00$^o$C |
| 10 | rtu_1_h2o | 7.00 g/kg | 1.40 g/kg |
| 11 | rtu_2_h2o | 9.00 g/kg | 1.80 g/kg |
| 12 | rtu_ 3_h2o | 9.00 g/kg | 1.80 g/kg |
| 13 | rtu_4_h2o | 9.00 g/kg | 1.80 g/kg |
| 14 | rtu_1_mass | 2.9320 kg/s | 0.5864 kg/s |
| 15 | rtu_2_mass | 0.5320 kg/s | 0.1064 kg/s |
| 16 | rtu_3_mass | 0.3990 kg/s | 0.0798 kg/s |
| 17 | rtu_4_mass | 0.5320 kg/s | 0.1064 kg/s |
| 18 | load_dining | 1.00 | 0.20 |
| 19 | load_winebar | 1.00 | 0.20 |
| 20 | kitchen_inflow_temp | 25.00$^o$C | 5.00$^o$C |
| 21 | kitchen_inflow_h20 | 16.00 g/kg | 3.20 g/kg |
| 22 | kitchen_inflow_mass | 0.5910 kg/s | 0.1180 kg/s |

Table 1. Input Variables: Nominal and Perturbation Values

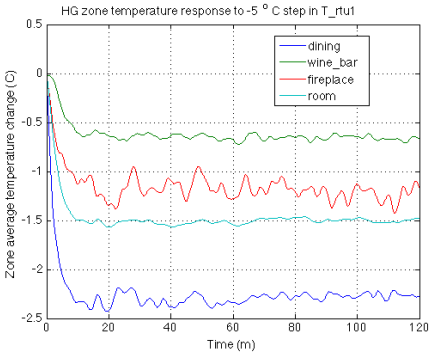


Fig. 4. Temperature responses to $-5^o$C change in RTU_1

## 4. INPUT VARIABLES

Twenty-two of the boundary conditions discussed in § 2.1 were identified as useful for injecting control or disturbance to the system. These are enumerated in Table 1. For each input we ran a FLUENT simulation beginning from the final state of the *steady* simulation and proceeding for 7200 s. In each run, one of the inputs in Table 1 was subjected to a ramp input beginning at $t = 8$ s, ramping to the appropriate perturbation value over 60 s, then remaining constant at the perturbed value.

## 5. SOME RESPONSE RESULTS

### *5.1 Response to RTU_1 (see Fig. 4)*

We now examine the FLUENT response to a $5^o$C decrease in the RTU_1 supply air. Since the **dining zone** is primarily served by RTU_1 it is reasonable that it exhibits the largest decrease ($\approx 2.3^o$C). The **wine_bar zone** which is mainly served by RTU's 2 & 4 exhibits a smaller decrease $\approx 0.6^o$C).

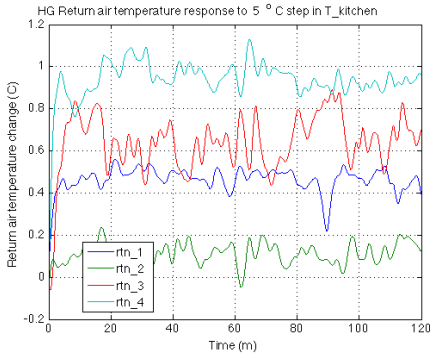


Fig. 5. Return air temperature response to $5^o$C increase in kitchen air temperature

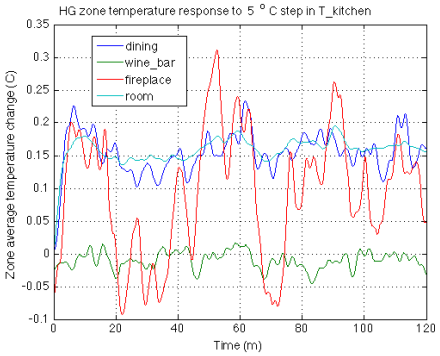


Fig. 6. Temperature response to $5^o$C increase in kitchen air temperature

### *5.2 Response to kitchen*

We now examine the FLUENT response to a $5^o$C increase in the air from the kitchen. This *kitchen* air flows into the domain through the red areas on the right side of Fig. 2; along the $\max x$ (South) wall. Fig. 5 displays the responses at the return air vents for the RTU's. As expected the largest effect is seen in rtn_4 which is closest to the kitchen. The **zone** temperature responses to the kitchen temperature increase are shown in Fig. 6. The effects on the **dining zone** and the **room** are about the same ($\approx 0.15^o$C increase). The **wine_bar zone** seems to have little response, and *on this scale* the **fireplace** temperature seems quite random. Note that the initial values for the wine_bar and the fireplace are non-zero. This accrues to the earlier observation that the $t = 0$ values are not close to the mean values computed over the last hour of nominally steady operation. We use the mean values as **nominal values** in defining the perturbations displayed in the figures. The **fireplace** response in Fig. 6 is problematic with variations ($\approx \pm 0.2^o$C) persisting throughout the response.

## 6. LTI MODEL

As noted in § 2 our approach is to construct an LTI model that approximates the perturbed CFD responses generated by FLUENT simulations. Whereas there are a number of approaches to extract reduced-order LTI models from response data (for example Kung (1978) and Gugercin (2008)), we are motivated to find a low order model with

| Number | Name | Value |
|---|---|---|
| 1 | q_north | 11.5095 w/m$^2$ |
| 2 | q_east | 10.4278 w/m$^2$ |
| 3 | q_west | 19.3538 w/m$^2$ |
| 4 | q_floor | 15.8151 w/m$^2$ |
| 5 | q_ceiling | 4.9463 w/m$^2$ |
| 6 | rtn_1_mass | −2.4959 kg/s |
| 7 | rtn_2_mass | −0.8248 kg/s |
| 8 | rtn_3_mass | −0.8248 kg/s |
| 9 | rtn_4_mass | −0.8392 kg/s |
| 10 | rtn_1_temp | 22.1082$^o$C |
| 11 | rtn_2_temp | 22.3562$^o$C |
| 12 | rtn_3_temp | 21.7175$^o$C |
| 13 | rtn_4_temp | 22.6413$^o$C |
| 14 | rtn_1_h2o | 9.3741 g/kg |
| 15 | rtn_2_h2o | 9.2538 g/kg |
| 16 | rtn_ 3_h2o | 9.2147 g/kg |
| 17 | rtn_4_h2o | 10.5528 g/kg |
| 26 | rtu1_z1_temp | 21.1414$^o$C |
| 27 | rtu2_z1_temp | 22.2903$^o$C |
| 28 | rtu3_z1_temp | 21.3036$^o$C |
| 29 | rtu4_z1_temp | 22.0641$^o$C |
| 34 | dining_room_temp | 21.9751$^o$C |
| 35 | dining_room_h2o | 9.2293 g/kg |

Table 2. Selected Nominal Steady Outputs

appropriate asymptotic behavior in a computationally efficient way.

### *6.1 Nominally Steady Outputs*

In order to describe perturbed responses in a meaningful way we first deal with defining *steady* values of the output variables.

It is clear from Fig. 3 that notable oscillations persist in the output variables. There are several potential explanations for this observed behavior:

(1) there is no guarantee that the Reynolds-Averaged Navier-Stokes PDE model has a steady solution;
(2) the grid may not be sufficiently resolved to represent the PDE behavior; and,
(3) the iterative procedure for the nonlinear algebraic system may not be sufficiently converged.

Whatever the cause(s) we simply define steady values for the outputs by averaging over a time-window. In particular, steady output values are computed by averaging the observed outputs over the final 60 minutes of the nominally steady solution. Steady values for the four output variables in Fig. 3 are indicated by the solid lines. Steady values for selected output variables are listed in Table 2.

### *6.2 CFD Perturbations*

For each of the twenty-two inputs (see Table 1) we ran a FLUENT simulation beginning from the final state of the *steady* simulation and proceeding for an additional 7200 s. In each run, one of the inputs in Table 1 was subjected to a ramp input beginning at $t = 8\,\mathrm{s}$, ramping to the appropriate perturbation value over 60 s, then remaining constant at the perturbed value. In each case the output variables (see Table 2) were recorded at 4 s intervals (1800 samples). For each input perturbation perturbed output values were computed as:

$$y_{\mathrm{pert}}(t_\jmath) = Y_{\mathrm{data}}(t_\jmath) - Y_{\mathrm{nom}} \quad \jmath = 1, ..., 1800 \ .$$

### *6.3 Best Fit*

There are several elegant approaches to extracting a model from time-response data (Kung (1978), Borggaard (2012) and Cliff (2012)). Our approach to computational efficiency begins by decomposing the problem into subproblems by treating each input response separately. That is, we hypothesize a structure for a low-order model and formulate an optimization problem to find appropriate parameter values. Specifically, for each input we propose a first-order model

$$\dot{x}(t) = -\frac{1}{\tau}x(t) + b\,u(t) \tag{2}$$

$$y(t) = C\,x(t) + D\,u(t)\ , \tag{3}$$

where $b$ is scalar, and $C, D \in \mathbb{R}^{43}$. We take $b = 0.01$ (scaling). Most of the $22 \times 43$ input/output pairs are represented as strictly-proper transfer functions ($D = 0$). However, for the first five inputs (surface temperatures) the heat flux output for that surface has a single non-zero entry in $D$. This can be seen in the usual convective cooling expression (1). The surface temperature is directly coupled to the heat flux on that surface. Thus, we expect that for surface heat flux outputs (the first five) we have $D^\jmath = h\delta_{\imath\,\jmath}$, whereas for all other outputs we have $D = 0$.

The time-scales of the building envelope are typically much longer than that of the indoor-air, so that during much of the response the indoor-air system will be near equilibrium. For this reason we require that the ROM accurately represent the near equilibrium response of the indoor-air dynamics. This requirement is not naturally imposed in other methods and leads to our *ad-hoc* approach. Since the input perturbation function $u$ goes to a constant value (say, $u_{\mathrm{ss}}$), then with $\tau > 0$ the dynamics (2) will go to the stable equilibrium

$$x_{\mathrm{ss}} = \tau\,b\,u_{\mathrm{ss}} \Rightarrow y_{\mathrm{ss}} = (C\,\tau\,b\ +\ D)\,u_{\mathrm{ss}}\ .$$

Solving for $C$ we find

$$C(\tau, D) = \frac{y_{\mathrm{ss}}/u_{\mathrm{ss}} - D}{\tau\,b}\ , \tag{4}$$

where the vector $D \in \mathbb{R}^{43}$ has (at most) a single non-zero entry. To implement (4) we must specify a method for computing a steady-state value of the perturbed output, *i.e.* $y_{\mathrm{ss}} \in \mathbb{R}^{43}$. Because the output data includes residual oscillations it is prudent to use some form of averaging. For the results presented here we averaged $y(t_\imath)$ over the last 120 samples (out of 1800 total), that is $\imath \in \{1681, 1682, ...1800\}$. This amounts to an 8 minute wide sampling window.

With these preliminaries we define a scalar-valued error function

$$J(\tau, D) = \sum_{\imath=1}^{1800} \left[y_{\mathrm{pert}}(t_\imath) - y(t_\imath; \tau, D)\right]^2\ , \tag{5}$$

where $y(t_\imath; \tau, D)$ is computed from (2, 3) with the state-to-output map given by (4), and the input ($u$) is the step-like input described in § 6.2. For each input we compute optimal values of $\tau$ and (possibly) $D$ by minimizing the error functional $J$ in (5). These calculations were done using MATLAB's `fminsearch` procedure.

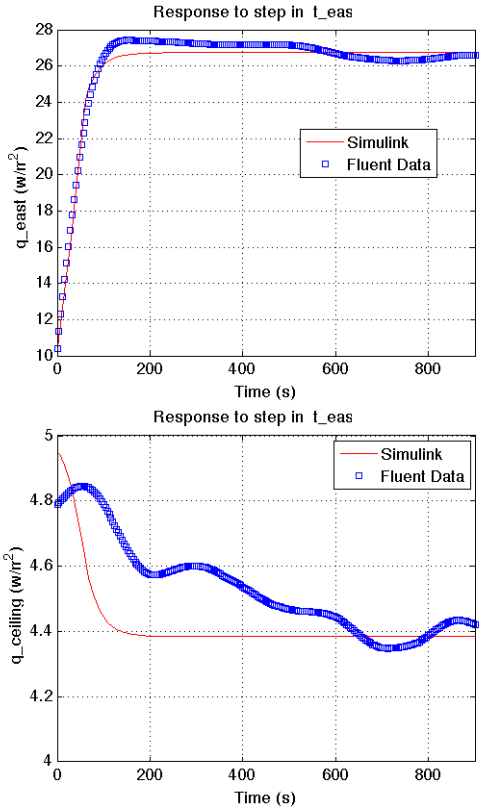


Fig. 7. FLUENT ROM comparison of T_east responses

The five non-zero values for the $D$ arrays are;

(1) q_north: 2.912 $\mathrm{w/m^2/^oC}$
(2) q_east: 2.038 $\mathrm{w/m^2/^oC}$
(3) q_west: 3.514 $\mathrm{w/m^2/^oC}$
(4) q_floor: 4.281 $\mathrm{w/m^2/^oC}$
(5) q_ceiling: 1.423 $\mathrm{w/m^2/^oC}$

Note that these can be interpreted as (time and spatial) averages of the film cooling coefficient on the respective surfaces.

## 7. ROM-FLUENT COMPARISONS

Fig. 7 provides comparisons of the FLUENT and the reduced-order-model (ROM) responses to a change in the east wall temperature. The input perturbation ramps to $+5^oC$ over 60 s and the corresponding ramp in the East wall heat flux is seen in the upper graph. In the lower graph the ceiling heat flux is seen to decrease by $0.6\mathrm{w/m^2}$, presumably the result of the increase in the air temperature engendered by the increased wall temperature. Note that the graphs display only the first 15 minutes of the response; the data fits are based on two hours of data.

Similarly, Fig. 8 provides comparisons of the FLUENT and the reduced-order-model (ROM) responses to a $5^oC$ decrease in the RTU#1 supply temperature. The upper graph displays the change in return air temperature, whereas the lower graph characterizes the temperature in the dining zone.

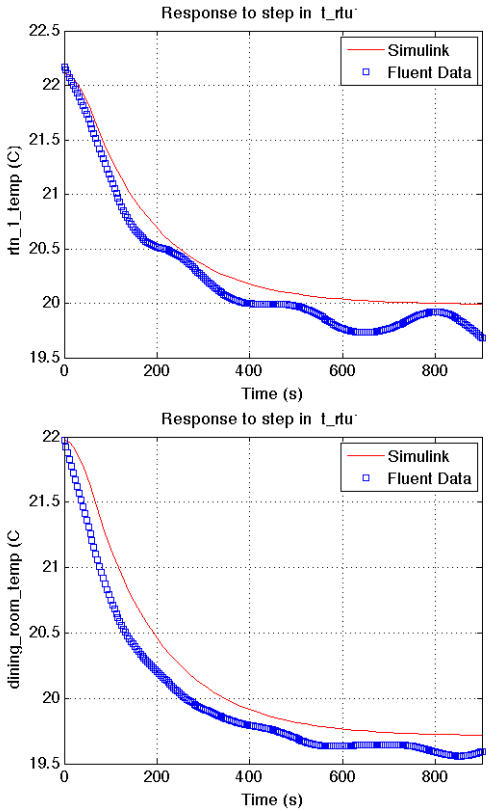


Fig. 8. FLUENT ROM comparison of T_rtu_1 responses

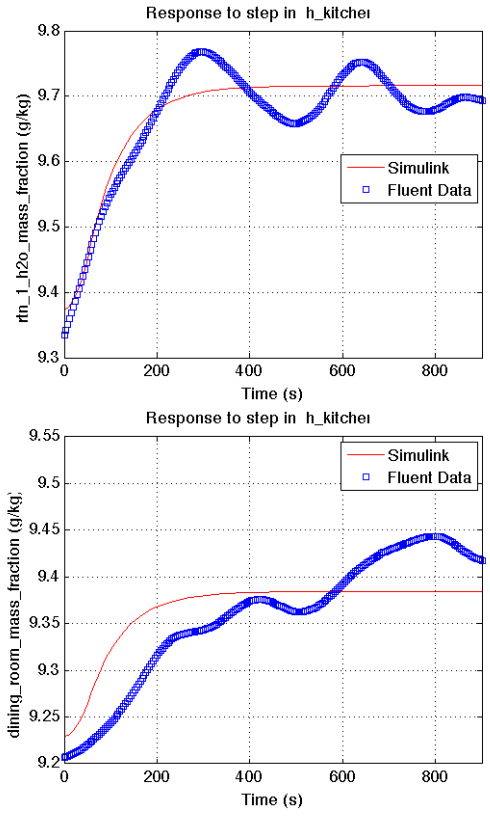


Fig. 9. FLUENT ROM comparison of h_kitchen responses

Finally, Fig. 9 displays responses to a 20% increase in the moisture mass fraction of the air flowing from the kitchen. This is a disturbance input in the model; a good controller will compensate to maintain comfortable conditions in the occupied areas.
Note that some of these comparisons appear very accurate while others exhibit discrepancies over longer time periods. In most cases, we see a roughly 5% relative difference in the responses between the ROM and the Fluent training data. Some of the Fluent responses from the ramp input contain significant oscillations, while these oscillations cannot be captured given the simplified form of the indoor-air models (2)-(3). However, in practice, the inputs from envelope vary much slower than those inputs used here to excite the internal dynamics in the Fluent datasets. Therefore, *if* we had access to a stable steady-state solution as an initial condition, forcing Fluent from the envelope model would not likely result in such oscillatory behavior in these outputs. While more research needs to be done to compute more accurate ROMs for energy efficient buildings, the ROM for indoor-air environment considered here captures the essential behavior of the flow and is certainly efficient enough to be utilized in an online optimal control strategy.

## 8. ENVELOPE MODELING

As noted in the *Abstract*, an overall model for the cooling problem would couple the indoor-air model to models for the building envelope and for the mechanical equipment. Here we introduce simple models for these components.
We consider a simple envelope model including three major features:

- Exterior surfaces: representative of the four room walls and the ceiling.
- Thermal storage: characterized with high thermal capacitance and representative of the room floor.
- Room air: represented by the ROM.

The energy exchange mechanisms in this model are:

- Conduction through the external wall: $Q_{\text{cond}}$
- Convection from the exterior surfaces to the indoor air: $Q_{\text{conv}-\text{w}}$
- Convection from the storage (floor) to the indoor air: $Q_{\text{conv}-\text{s}}$

The lumped model resulting from these thermal exchanges gives two differential equations governing the wall and the storage temperatures. The equations are the following:

$$C_{\text{w}} \frac{\mathrm{d}T_w}{\mathrm{d}t} = -(Q_{\text{cond}} + Q_{\text{conv}-\text{w}}) \tag{6}$$

$$C_{\text{s}} \frac{\mathrm{d}T_s}{\mathrm{d}t} = -Q_{\text{conv}-\text{s}} \tag{7}$$

where $C_{\text{w}}$ and $C_{\text{s}}$ are respective thermal capacitances of the wall and the storage and the energy flows are given by:

$$Q_{\text{cond}} = \frac{k_{\text{w}}(A_{\text{north}} + A_{\text{east}} + A_{\text{west}} + A_{\text{ceiling}})}{\Delta_{\text{w}}}(T_{\text{w}} - T_{\text{e}})$$

$$Q_{\text{conv}-\text{w}} = A_{\text{north}}\, q_{\text{north}} + A_{\text{east}}\, q_{\text{east}} + A_{\text{west}}\, q_{\text{west}} + A_{\text{ceiling}}\, q_{\text{ceiling}}$$

$$Q_{\text{conv}-\text{s}} = A_{\text{floor}}\, q_{\text{floor}}$$

$A$ here stands for area, $q$ for flux, $k$ for thermal conductivity, $\Delta$ for thickness and $T_{\text{e}}$ for prescribed external temperature. In summary, the envelope model can be summarized in:

$$\dot{z}(t) = Jz(t) + B(t)\ , \tag{8}$$

where $z = [T_{\text{w}}, T_{\text{s}}]^T$, $J$ and $B$ may be deduced from previous discussions. Note that the temperatures $T_{\text{w}}, T_{\text{s}}$ are inputs to the ROM and that $B$ incorporates output terms from the ROM (surface heat fluxes).

## 9. OPTIMAL CONTROL

In order to optimize the cooling energy used during a summer day, we use Model Predictive Control (MPC) on the coupled ROM-Envelope model illustrated in Fig. 10. The occupancy and kitchen loads, RTU supply temperatures from the different zones, which are the control variables, and the wall temperatures computed from the envelope model are fed into the ROM. To compute these wall temperatures, the envelope model needs the external weather temperature and the wall fluxes computed from the ROM. The cost function which is the cooling energy cost and the comfort constraints are discussed later.

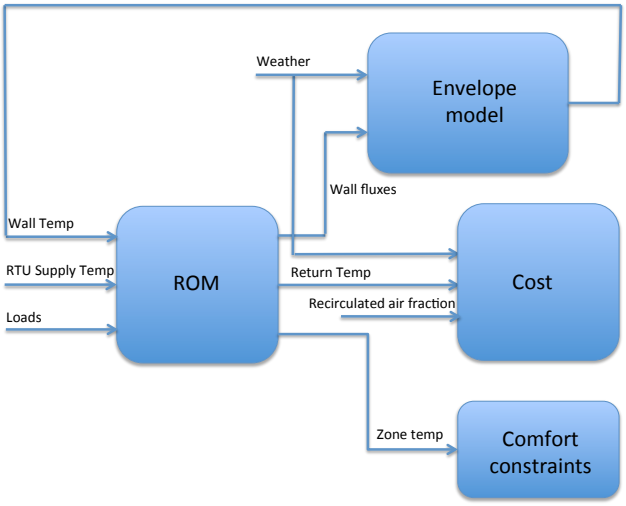


Fig. 10. Simplified scheme of ROM-envelope coupling

### 9.1 Cost Function (Equipment Model)

The expression of the power used for the cooling coil is inspired by the formulation of Kelman (2011).

$$Pc = \sum_{i=1}^{4} \frac{Cp}{cop_i} \dot{m}_i (Tm_i - Tc_i) \tag{9}$$

Where the subscript $i$ designates quantities related to the $i^{th}$ RTU, $Cp$ is the heat capacity of the air at constant temperature, $cop_i$ is the cooling coefficient of performance, $\dot{m}_i$ is the nominal supply mass flow rate, $Tm_i$ is the RTU inlet air temperature and $Tc_i$ is the supply RTU temperature. The RTU inlet air temperature or the mixing temperature can be written as:

$$Tm_i = (1 - d_r)T_e + d_r Tr_i \quad (10)$$

where $d_r$ is the fraction of supply flow recirculated from zones, $T_e$ is the outside air temperature and $Tr_i$ is the return temperature at each zone.
The final cost expression can be written as:

$$C = \int_0^T (P_c)dt \quad (11)$$

where $T$ is a 24-hour period.

### 9.2 Constraints

Most of the constraints are applied for each RTU i (i=1, 2, 3, 4):

(1) Specify upper and lower bounds for the control temperature for different RTUs. $10^oC \leq Tc_i \leq 30^oC$
(2) Set upper comfort bound for the local temperature of the different zones at the occupancy time. For $h_{min} \leq t \leq h_{max}$, $T_a \leq 23^oC$.
(3) Set upper comfort bound for the average zone temperature at the occupancy time. For $h_{min} \leq t \leq h_{max}$, $T_a \leq 23^oC$.
(4) Cooling coil can only decrease temperature.
$$Tc_i \leq Tm_i$$
(5) Set upper and lower bounds for the recirculated air fraction. $0 \leq d_r \leq 0.9$
(6) Set upper and lower bounds for the cooling power of each RTU. $0 \leq Cp(\dot{m}_i)(Tm_i - Tc_i) \leq Cap_{max-i}$

### 9.3 Numerical Approximation

In model predictive control one is concerned with minimizing the functional (11) from a given initial state over a forward planning horizon ($[0, T]$). Here we briefly study a discretized version of the problem using the MATLAB/SIMULINK based tool: Berkeley Library for Optimization Modeling. At this time BLOM 2.0 is restricted to discrete-time dynamics, so it is necessary to convert from continuous to discrete time model. Thus, for example, the envelope model (8) is replaced by

$$z_{k+1} = \Phi z_k + \Gamma B_k \quad (12)$$

where $\Phi = \exp(J\delta t)$ with $\delta t$ is the time step (equal to 7.5 minutes here).

### 9.4 Numerical Results

The RTU properties are shown in Table 3 and the details of the loads are the following:

- Kitchen temperature: $25^oC$ rising to $28^oC$ between $t = 10am$ and $t = 10pm$.
- Dining load: 0.2 rising to 1.2 between $t = 12pm$ and $t = 10pm$.
- Wine bar load: 0.2 rising to 1.2 between $t = 12pm$ and $t = 10pm$.
- Occupancy: occupancy function is 1 between $h_{min} = 11am$ and $h_{max} = 10pm$, and 0 otherwise

We present the optimization results in the following figures. From these figures plotting the average zone temperature (Fig. 11), the local zone temperatures (Fig. 12), the control temperatures (Fig. 13), the fraction of recirculated air (Fig. 14) and the power used in each RTU (Fig. 15), we conclude the following. The control process can be divided into three regions: the first is from 0h to 11h where the comfort constraints are not active, the second is from 11h to 22h where the comfort constraints are active, and the third is from 22h to 24h where the comfort constraints are not active again. Concerning the first portion, all the units are off, and the mixing temperature is equal to the outside temperature. About the beginning of the occupancy period, the RTUs start to cool the area and the mixing temperature remains equal to the outside temperature which is still low compared the inside air temperature. At about 13h, the outside air temperature becomes higher then the return temperature. That influences almost all time histories which show an obvious discontinuity. In fact, the fraction of recirculated air jumps from 0 to 0.9 and the mixing temperature becomes mainly dependent on the return temperature at each zone. During this period, RTU 1 delivers greater levels of power than the other RTUs since it is the most efficient. It is also noticed that the use of RTU 3 is not efficient at all as shown in Fig. 15. Concerning the last period, the comfort constraints are relaxed which drives the power to return to zero at about 22h.

| RTU | $Cap_{max-i}$ | $cop_i$ |
|---|---|---|
| 1 | 53 kW | 3.5 |
| 2-4 | 14 kW | 2.6 |

Table 3. Properties of the RTUs in Harvest Grill

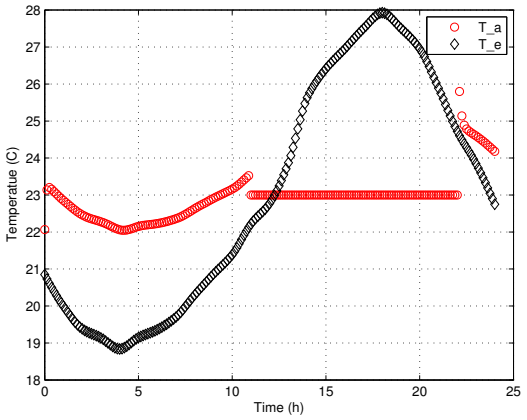


Fig. 11. Average zone temperature profile compared to the outside temperature

## 10. CONCLUDING REMARKS

A CFD-based ROM for the indoor-air has been coupled to a simple building envelope problem and used to formulate a minimum energy control problem. The BLOM software was a useful tool to formulate and solve a discrete-time version of the optimal control problem. Further studies with more detailed envelope and equipment models are presently being studied.

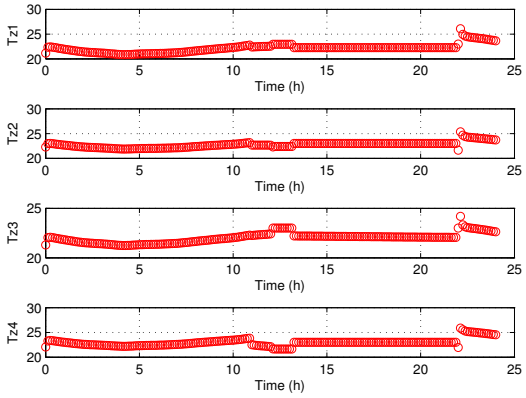


Fig. 12. Local zone temperatures

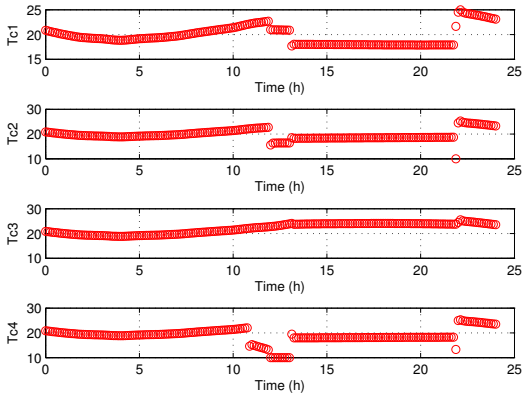


Fig. 13. RTU control temperatures

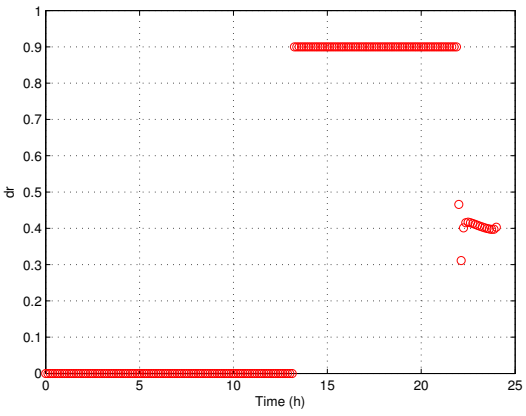


Fig. 14. Fraction of recirculated air

ACKNOWLEDGEMENTS

This research was supported in part by the Air Force Office of Scientific Research grant FA9550-10-1-0201 and by DOE contract DE-EE0004261 under subcontract # 4345-VT-DOE-4261 from Pennsylvania State University. Much of the data for the model was provided by D. Kim, A. Hjortland, and J.E. Braun of the Herrick Laboratory at Purdue University. Insights concerning Energy-Plus were

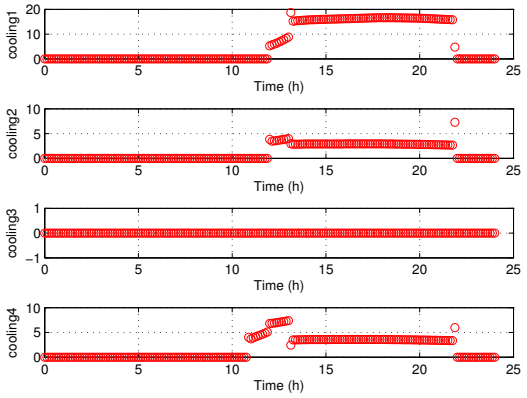


Fig. 15. Cooling used in each RTU

graciously provided by Prof. Z. O'Neill of the Mechanical Engineering Department at the University of Alabama. The authors also acknowledge the BLOM developers for the details they have provided about the library.

REFERENCES

Borggaard, J., Cliff, E., and Gugercin, S. (2012). Model reduction for indoor-air behavior in control design for energy-efficient buildings, *Proceedings of 2012 ACC*, 2012

Cliff, E.M., Borggaard, J.T., Braun, J.E., Gugercin, S., and Kim, D. (2012). Coupled CFD/building envelope model for the Purdue Living Lab, *2012 International High Performance Buildings Conference at Purdue*, Purdue University, West Lafayette, IN.

Gugercin, S., Antoulas, A.C., and Beattie, C.A. (2008). $\mathcal{H}_2$ model reduction for large-scale linear dynamical systems', *SIAM J. on Matrix Analysis*, 30, pages 609-638, 2008.

Kelman, A., and Borrelli, F. (2011). Bilinear model predictive control of a HVAC system using sequential quadratic programming, *P*roc. 18th IFAC World Congress, 2011

Kung, S.Y. (1978). A new identification and model reduction algorithm via singular value decomposition, *Proc. 12th Asilomar Conf. Circuits, Syst. Comput.*, 1978

Ma, Y., Kelman, A., Daly, Y., and Borrelli, F. (2012). Predictive control for energy efficient buildings with thermal storage, *IEEE Control Systems Magazine*, *DOI 10.1109/MCS.2011.2172532.*

Srebric, J., Chen, Q., and Glicksman, L.G. (2000). A coupled airflow-and-energy simulation program for indoor thermal environmental studies, *ASHRAE Transactions*, 106(1), pages 465-476.

Zhai, Z., Chen, Q., Hayes, P., and Klems, J. (2002). On approaches to couple energy simulations and computational fluid dynamics programs, *Building and Environment*, 37, pages 857-864.